A simple sequential-binding model for calcium puffs

D. Swaminathan,[1] G. Ullah,[2] and P. Jung[1]
[1]*Department of Physics and Astronomy and Quantitative Biology Institute, Ohio University, Athens, Ohio 45701, USA*
[2]*Department of Engineering Science and Mechanics, Center for Neural Engineering, Pennsylvania State University, University Park, Pennsylvania 16802, USA*

(Received 26 February 2009; accepted 19 May 2009; published online 18 September 2009)

Calcium puffs describe the transient release of Ca^{2+} ions into the cytosol, through small clusters of 1,4,5-inositol triphosphate (IP_3) receptors, present on internal stores such as the endoplasmic reticulum. Statistical properties of puffs, such as puff amplitudes and durations, have been well characterized experimentally. We model calcium puffs using a simple, sequential-binding model for the IP_3 receptor in conjunction with a computationally inexpensive point-source approximation. We follow two different protocols, a sequential protocol and a renewal protocol. In the sequential protocol, puffs are generated successively by the same cluster; in the renewal protocol, the system is reset after each puff. In both cases for a single set of parameters our results are in excellent agreement with experimental results for puff amplitudes and durations but indicate puff-to-puff correlations for the sequential protocol, consistent with recent experimental findings [H. J. Rose, S. Dargan, J. W. Shuai, and I. Parker, Biophys. J. **91**, 4024 (2006)]. The model is then used to test the consistency of the hypothesized steep Ca^{2+} gradients around single channels with the experimentally observed features of puff durations and amplitudes. A three-dimensional implementation of our point-source model suggests that a peak Ca^{2+} concentration of the order of 10 μM at the *cluster site* (not channel) is consistent with the statistical features of observed calcium puffs. © *2009 American Institute of Physics*.
[DOI: 10.1063/1.3152227]

Ca^{2+} ions play a vital role in numerous cellular regulatory mechanisms at all stages of a living organism. Life starts with a massive calcium wave roaming the fertilized egg cell and triggering embryonic development; calcium waves in heart cells regulate the strength at which these cells contract and how hearts beat; calcium signals in neurons facilitate their communication and hence our brain's ability to function. Yet, in spite of its great relevance for physiology, there are gaps in our quantitative understanding of the biophysical processes underlying calcium signaling. In this paper we focus on the most elemental form of calcium dynamics, the release of calcium from intracellular stores through small groups of release channels, a process on the micrometer scale. Since all forms of calcium signaling are built from these events it is worthwhile to quantitatively understand the biophysical processes underpinning these elemental events. The endoplasmic reticulum (ER) is an intracellular calcium rich source, with calcium values ranging up to 500 μM. The cytosolic concentration, however, is quite small and of the order of nanomolars. Hence, when small groups of ion channels (the gatekeepers of calcium) on the membrane of the ER open, a large amount of calcium rushes into the cytosol and increases the concentration in the vicinity of these channels. When the channels close, the spatially and temporally limited event, we call a calcium puff, terminates. We propose a simple and computationally inexpensive sequential model for these elemental calcium puffs, which reproduces the features of the experimentally observed ones well. Such a model can be used to large-scale simulations of cells where numerous of these elemental events give rise to waves and oscillations. We use this model to explore puff-to-puff correlations for puffs generated by the same cluster and to constrain peak calcium concentrations near the clusters of release channels.

I. INTRODUCTION: CALCIUM PUFFS

Calcium signaling is one of the most important cellular signaling mechanisms. It describes the transient increase in cytosolic calcium through release of calcium ions from intracellular stores or through plasma membrane channels. The shape of these signals varies widely in time and space, ranging from brief localized events of a few milliseconds to waves roaming the entire cell and even tissue such as liver, heart, and brain.

In this paper we focus on the most elemental calcium signaling event, termed the calcium puff. Calcium is stored in intracellular stores, most notably the ER and the sarcoplasmic reticulum. The concentration there is of the order of tens to hundreds of micromolars, much larger than in the cytosol where it is in the range of tens to several hundreds of nanomolars (see, e.g., Ref. 1). Calcium ions, Ca^{2+}, are released from stores through clusters of release channels with 10–30 channels each. The opening of these channels is determined in a large part by the cytosolic calcium concentration and by the presence of an additional second messenger, inositol trisphosphate (IP_3), which is generated upon binding

of extracellular agonist (e.g., hormones, neurotransmitter). Increased cytosolic Ca^{2+} increases the open probability of release channels (IP_3Rs). Hence, Ca^{2+} released from one open channel into the cytosol increases the open probability of other channels in the same cluster, leading to collective positive feedback and a rapid rise in the local cytosolic Ca^{2+} level. The number of channels recruited this way into a calcium release event varies stochastically giving rise to statistical distributions of the amplitudes, durations, and intervals between Ca^{2+} release events. These calcium release events, termed *calcium puffs*, are terminated through a mechanism which is not fully understood but thought of as channel inhibition upon cytosolic Ca^{2+} binding to an inhibitory binding site.

Clusters of IP_3Rs in the oocyte are randomly distributed and about 3 μm apart on the average. This spatial organization of the IP_3Rs in small clusters is essential for the hierarchical organization of Ca^{2+} release events, ranging from the most elemental single-cluster events, i.e., puffs, to multicluster events where the Ca^{2+} release from one cluster triggers the firing of one or more nearby clusters leading to a spread of the increased cytosolic Ca^{2+} concentration and to intracellular Ca^{2+} waves, where clusters fire up like a chain of dominos.

In this paper, we consider puffs released from single clusters. A detailed quantitative characterization of puffs has been provided earlier by Yao *et al.*,[2] Parker *et al.*,[3] and Sun *et al.*[4] The rise of cytosolic Ca^{2+} is fast and peaks within 20 ms.[5] The subsequent decline of cytosolic Ca^{2+} is reported within a few hundred milliseconds with an average reported between 60 and 150 ms. Puff amplitudes obtained from experiments are averaged over a small domain of about 1 μm length. They are characterized by the statistical distribution of the maxima of these averages within one puff. The resulting puff-amplitude distributions are approximately Gaussian with a peak at about 200 nM and a small proportion of puffs having a much larger amplitude. A more skewed distribution is reported in Ref. 4. The lateral spread of Ca^{2+} away from the release site has been characterized as diffusive, with an effective diffusion coefficient of about 25 $\mu m^2/s$ and observed for a few microns.[4] The spatial spread of a puff ranges between 2 and 5 μm.[4]

Early studies reported values for the time intervals between puffs, at a single site, in the range of 10 s.[3] Later studies corrected these numbers to 3 s (Ref. 6) (at an IP_3 concentration of about 0.3 μM) and most recently to about 1 s.[7]

While the reported puff amplitudes are of the order of 0.1 μM, it has been hypothesized based on computational studies[8] that the Ca^{2+} concentrations in the vicinity of the channel pores are much larger, i.e., of the order 100 μM. Detailed numerical studies have confirmed these large local concentrations.[9,10] The large concentration of Ca^{2+} near the channels poses a significant computational problem which has been addressed with, e.g., sophisticated finite element techniques[10] if the model is to fully resolve the details of the concentration profile around the channel.

In this paper, similar in spirit to the recent study by Solovey *et al.*,[11] we propose a simple, computationally inexpensive model for calcium puffs, which generates puffs with frequencies, amplitudes, and durations consistent with experimental values. At the heart is a model for the gating of the IP_3 receptors which is derived from the DeYoung–Keizer model but incorporates sequential binding and a larger rate of inhibition. In the spirit of simplicity, we use a point-source model, which effectively describes the Ca^{2+} release from the ER through the entire cluster at a point. Such a model is obviously not designed to resolve Ca^{2+} profiles near single IP_3Rs and the possibly very steep Ca^{2+} concentration profiles, but it can be useful to address physiological questions on larger spatial scales such as the dynamics of Ca^{2+} patterns from the scale of micrometers upward which requires simulating a large number of clusters.

The key feature of a point-source model is that all channels of a cluster and all their binding sites experience the same value of the calcium concentration. But this concentration is not the large concentration generated by a single pore close to the pore; it is a concentration that represents an average value of calcium experienced by the binding sites of a channel when a representative number of channels are open. This value is not *a priori* known and will be constrained by observed statistical properties of puffs.

In Sec. II we describe our model and the computational methods we use to analyze it. Similar as in Refs. 12 and 13 we derive, through lumping of states, reductions of our six-state IP_3 receptor model to a four-state and a two-state model.

We then present results for puff characteristics using two different protocols, a *sequential protocol*, where puffs are generated continuously from one single cluster, and a *renewal protocol*, where the system is reset after each puff to a predefined state. We show that our model delivers puffs with statistical characteristics (duration and amplitude) consistent with those observed experimentally. Using the two different protocols, we identify correlations between subsequent puffs generated by a single cluster, which can be explained in a similar way as those observed in experiments[13] by channel inhibition. We further test the accuracies of the four-state and two-state model reductions.

Finally, we investigate the consistency of large Ca^{2+} concentrations around the cluster sites. First, we show that the two-dimensional implementation of our model, although its results are consistent with physiological values, is clearly inconsistent with steep Ca^{2+} gradients around the cluster sites. But we can reconcile this difference to an extent by using a three-dimensional (3D) implementation of the model giving rise to consistent puff amplitudes and durations for peak cluster concentration at around 10 μM.

II. THE MODEL

The spatiotemporal dynamics of the cytosolic Ca^{2+} concentration c is modeled by the following two-dimensional reaction diffusion equation:

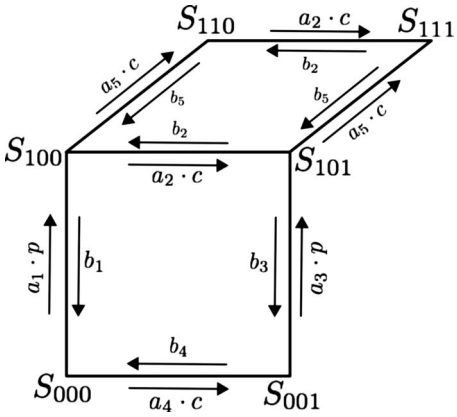

FIG. 1. A schematic diagram of the kinetics of a single IP_3 subunit for the six-state model. The transition rates between receptor states are indicated next to the arrows. p denotes the IP_3 concentration.

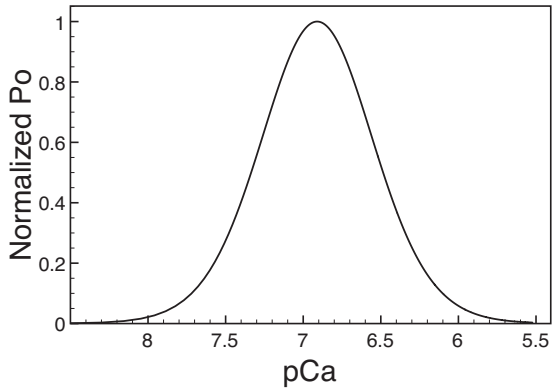

FIG. 2. Steady-state open probability curve for the six-state model at 2 μM IP_3. Calcium sensitivity peaks at 123 nM of $[Ca^{2+}]$. The open probability is normalized with respect to peak P_o value. pCa equals $-\log 10[Ca^{2+}]$.

$$\frac{dc}{dt} = D\nabla^2 c + \delta(\vec{x} - \vec{x}_0)J_{\text{cluster}} - J_{\text{pump}} + J_{\text{leak}}. \tag{1}$$

Here J_{cluster} denotes the flux of Ca^{2+} from the ER into the cytosol through one cluster of IP_3Rs containing a small number of channels, and $\vec{x}_0$ is the position of the point cluster. Each cluster comprises N channels and the total cluster flux is given by

$$J_{\text{cluster}} = N(\pi r_c^2)v_{\text{cluster}}\left(\frac{N_o}{N}\right)(\text{Ca}_{\text{er}} - [\text{Ca}^{2+}]), \tag{2}$$

where $r_c \approx 5$ nm denotes the radius of the channel and v_{cluster} determines the maximum flux. The number of open channels is simulated by using a stochastic version of the kinetic scheme of the IP_3 receptor as described in Sec. III.

As it is now well established that the IP_3R is a tetramer[14] we assume that the IP_3 receptor has four equal and independent subunits. Each subunit has three binding sites: an IP_3 binding site, a Ca^{2+} activation binding site, and a Ca^{2+} inhibition binding site, each of which is either occupied or unoccupied. Therefore, each subunit can exist in any of the eight permissible states. We make two assumptions. First, unlike the DeYoung–Keizer model[15] we force sequential binding of IP_3 and Ca^{2+} to the receptor. This means that Ca^{2+} only binds to the activation site on the subunit once IP_3 has bound to the subunit. In the absence of bound IP_3, Ca^{2+} does not bind to the activation site. Thus, if S_{ijk} denotes the state of a subunit, where i characterizes the state of the IP_3 binding site ($i=0$ means not bound), j the state of the Ca^{2+} activation binding site, and k the state of the inhibiting Ca^{2+} binding site, the two states S_{010} and S_{011} do not exist. Therefore we have a six-state model for each subunit of the IP_3R as opposed to the eight-state DeYoung–Keizer model. The subunit is activated only when the IP_3 and Ca^{2+} activation sites are occupied. The channel is considered open if any three or all four subunits are activated. Second, we increase the rate of inhibition by a factor of 10, reducing the mean open time of the channels. Figure 1 shows a schematic diagram for the receptor subunit.

Figure 2 shows the normalized steady-state open probability P_o of the receptor as a function of the Ca^{2+} concentration for a fixed IP_3 concentration of 2 μM. Similar to the protocol in Ref. 16 the open probabilities are normalized to its maximum value. Reported open probabilities of the IP_3 receptor range from <0.01 (Ref. 17) up to 0.5 (Ref. 18). For our model at 2 μM IP_3, the open probability peaks at around 0.042, with the peak at Ca^{2+} concentration of about 120 nM. The peak Ca^{2+} sensitivity correlates well with data published by Tu *et al.*[16] On cell membranes, three different types of IP_3 isoforms are known to exist. At 2 μM IP_3, Tu *et al.*[16] measured peak Ca^{2+} sensitivity for P_o to be at 257 nM of Ca^{2+} for type 1 isoform, 154 nM of Ca^{2+} for type 2 isoform, and 107 nM of Ca^{2+} for type 3 isoform. We therefore conclude that our model operates within a physiologically relevant range.

Our approach for the IP_3R is not meant as a substitute for detailed and realistic models of the IP_3 receptor[19–21] designed to further our understanding of these receptors. Our target is to arrive at a model that is computationally efficient and accurate on the organizational scale of puffs and waves.

In the spirit of simplicity we do not incorporate buffers explicitly but use the effective diffusion coefficient $D = 25$ $\mu m^2/s$ extracted from data,[4] and therefore incorporates the role of buffers. As it is essential to restore low cytosolic Ca^{2+} concentrations, once Ca^{2+} is released into the cytosol, the cell recruits the sarcoendoplasmic reticulum calcium ATPases (SERCA or calcium pumps) present on the ER membrane for the reuptake of Ca^{2+} from the cytosol. We assume the SERCA pumps to be distributed uniformly on the ER membrane and model the pump flux J_{pump} with a Hill coefficient of 2, i.e.,

$$J_{\text{pump}} = \frac{v_{\text{pump}}[\text{Ca}^{2+}]^2}{k_{\text{pump}}^2 + [\text{Ca}^{2+}]^2}. \tag{3}$$

The remaining term $J_{\text{leak}} = v_{\text{leak}}(c_{\text{ER}} - c)$ describes nonspecific Ca^{2+} leakage from the ER into the cytosol.

The Ca^{2+} concentration in the ER is much larger than the cytosolic Ca^{2+} and is assumed to be constant, i.e., the possibility of store depletion is neglected here. Table I lists the values of all model parameters. Detailed balance has been imposed with $k_1k_2 = k_3k_4$, k_i being the ratio of the receptor dissociation constant to the receptor association constant.

TABLE I. Model parameters.

Parameter	Value	Description
$v_{cluster}$	5689.0 s^{-1}	Max. $[Ca^{2+}]$ channel flux
v_{leak}	0.020 35 s^{-1}	$[Ca^{2+}]$ leak flux constant
v_{pump}	45.5 $\mu M\ s^{-1}$	Max. $[Ca^{2+}]$ uptake
k_{pump}	0.1 μM	Activation constant for $[Ca^{2+}]$ pump
D	25.0 $\mu m^2\ s^{-1}$	Effective diffusion coefficient of cytosolic $[Ca^{2+}]$
	Receptor binding constants	
a_1	167.6 $(\mu M\ s)^{-1}$	IP_3
a_2	3.81 $(\mu M\ s)^{-1}$	Ca^{2+} inhibition
a_3	413.4 $(\mu M\ s)^{-1}$	IP_3
a_4	0.3101 $(\mu M\ s)^{-1}$	Ca^{2+} inhibition
a_5	53.9 $(\mu M\ s)^{-1}$	Ca^{2+} activation
	Receptor dissociation constants	
b_1	228.0 s^{-1}	IP_3
b_2	0.409 s^{-1}	Ca^{2+} inhibition
b_3	188.5 s^{-1}	IP_3
b_4	0.096 s^{-1}	Ca^{2+} inhibition
b_5	4.52 s^{-1}	Ca^{2+} activation

The maximum pump flux v_3 in conjunction with the luminal Ca^{2+} is the main determinant of the basal Ca^{2+} concentration in our model.

We solve the partial differential equation [Eq. (1)] on a square area of $5\times5\ \mu m^2$ using a four-point discretization of the Laplacian and a fully explicit solver. Boundary conditions are such that no flux can enter the square area. The δ function in Eq. (1), modeling a point cluster, is implemented in discrete fashion by (a) limiting the flux to a bin with area $dxdy$, where dx and dy are the discretization intervals, and (b) dividing the total flux by the bin area $dxdy$ such that the integral over the cluster is independent of the bin size. 3D simulations of this nature involve a cubic volume being simulated using a six-point discretization of the Laplacian and a fully explicit solver. Yet, it is important to realize that the computationally efficient point-source method comes with a disadvantage: Decreasing the discretization length leads to a decreased source size and hence a larger flux density and correspondingly, a modified local peak concentration which in turn can affect the gating of the channels. This effect, however, is weak unless the bin size becomes much smaller than the estimated cluster size of $40\times40\ nm^2$. To resolve such spatial detail a distributed source model will be necessary (see, e.g., Ref. 22). On the other hand, the point-source model still gives reasonably accurate results for a discretization length as large as 100 nm, similar as reported in Ref. 11. Unless stated differently, we use a bin size of $50\times50\ nm^2$, close to the actual size of a cluster.

For the stochastic simulation of the IP_3 receptor, we assume that all subunits are independent and that each subunit of the receptor undergoes stochastic transitions between its states, through stochastic association and dissociation of the agonist (see also the recent review in Ref. 23). Transition rates between states depend on the agonist binding rates (see Fig. 1) and for a sufficiently small time step, transition probabilities have a linear dependence on the time step. Specifically, if a subunit is in state A_i and has access to states A_j with transitions rates r_{ij}, the probability of a transition $i\rightarrow j$ is given by $r_{ij}dt$ with dt small enough that $r_{ij}dt\ll1$ and the probability to remain in state A_i is $1-\Sigma_j r_{ij}dt$. We randomly select from these transitions with a weight proportional to their probabilities.

A. Quasi-steady-state reductions

The full set of rate equations describing a subunit of an IP_3 receptor, introduced above, reads (see also Fig. 1)

$$\begin{aligned}
\frac{dx_{000}}{dt} &= b_1x_{100} + b_4x_{001} - (a_1p + a_4c)x_{000},\\
\frac{dx_{001}}{dt} &= b_3x_{101} + a_4cx_{000} - (b_4 + a_3p)x_{001},\\
\frac{dx_{100}}{dt} &= a_1px_{000} + b_2x_{101} + b_5x_{110} - (b_1 + a_5c + a_2c)x_{100},\\
\frac{dx_{101}}{dt} &= b_5x_{111} + a_2cx_{100} + a_3px_{001} - (a_5c + b_2 + b_3)x_{101},\\
\frac{dx_{110}}{dt} &= b_2x_{111} + a_5cx_{100} - (a_2c + b_5)x_{110},\\
\frac{dx_{111}}{dt} &= a_5cx_{101} + a_2cx_{110} - (b_5 + b_2)x_{111},
\end{aligned} \tag{4}$$

where x_{ijk} denote the probabilities for a subunit to be in states S_{ijk}, respectively.

We now proceed to employ quasi-steady-state approximations by exploiting time scale separation of the full six-state model. It should be pointed out that the actual separation of time scales of various rate processes depends on the Ca^{2+} concentration and is for our model and its parameter values only valid for calcium concentrations up to around 1 μM, i.e., for relatively small values of v_1. It is this regime we are considering below.

In the first reduction we exploit the fact (similar as in Ref. 12) that IP_3 binding and dissociation is faster than the other competing processes by assuming that the transitions between the states x_{1ij} and x_{0ij} are equilibrized, i.e.,

$$b_jx_{1ik} = a_jpx_{0ik}, \quad j=1,3,\ \ i,k=0,1, \tag{5}$$

where p denotes the IP_3 concentration. We exploit this relation to reduce our six-state model to a four-state model by lumping together states x_{0ik} and x_{1ik} into states X_{ik}. In this reduced model, the subunit conducts in the X_{10} state. The set of six differential equations, that govern the subunit dynamics for a six-state model, following the approximation reduces to the following set of four equations (for a graphical scheme, see Fig. 3):

$$\frac{dX_{00}}{dt} = \frac{b_4\kappa_3 + b_2}{1+\kappa_3}X_{01} + b_5X_{10} - \frac{(a_4\kappa_1 + a_5 + a_2)}{1+\kappa_1}cX_{00},$$

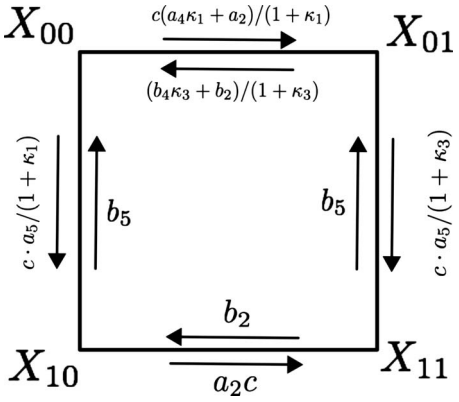

FIG. 3. A schematic diagram of the kinetics of a single IP_3 subunit for the four-state model. The modified transition rates in between receptor states are as shown in the figure.

$$\frac{dX_{10}}{dt} = b_2X_{11} + \frac{a_5}{1+\kappa_1}cX_{00} - (a_2c+b_5)X_{10},$$

$$\frac{dX_{01}}{dt} = \frac{a_4\kappa_1+a_2}{1+\kappa_1}cX_{00} + b_5X_{11} - \frac{b_4\kappa_3+b_2+a_5c}{1+\kappa_3}X_{01}, \tag{6}$$

$$\frac{dX_{11}}{dt} = \frac{a_5}{1+\kappa_3}cX_{01} + a_2cX_{10} - (b_5+b_2)X_{11},$$

where

$$\kappa_j = \frac{b_j}{a_jp}, \quad j=1,3. \tag{7}$$

In a second reduction, we start from the four-state model [Eq. (6)] and lump states again, i.e.,

$$Y_k \equiv \sum_{i,k=0}^{1} X_{ik} = Y_k, \tag{8}$$

yielding a two-state approximation for each subunit with the activated state Y_0 and the inhibited state Y_1, i.e.,

$$\frac{dY_0}{dt} = \frac{(b_4\kappa_3+b_2)\kappa_5+b_2}{(1+\kappa_3)\kappa_5+1}Y_1 - \frac{(a_4\kappa_1+a_2)\kappa_5+a_2}{(1+\kappa_1)\kappa_5+1}cY_0,$$

$$Y_1 = 1-Y_0, \quad \kappa_5 = \frac{b_5}{a_5c}. \tag{9}$$

Before we use the stochastic version of this reduced four-state model, we compare the bifurcation diagrams of the corresponding rate equations for the full six-state [Eq. (4)] and four-state models [Eq. (6)] (Fig. 4) with the IP_3 concentration as a bifurcation parameter. We replace J_{cluster} by

$$J_{\text{channel}}^{\text{six state}} = v_1(4x_{110}^3(1-x_{110}) + x_{110}^4)(c_{\text{er}}-c),$$

$$J_{\text{channel}}^{\text{four state}} = v_1(4X_{10}^3(1-X_{10}) + X_{10}^4)(c_{\text{er}}-c), \tag{10}$$

respectively. In Fig. 4, we depict the bifurcation diagrams for the full six-state model, the four-state model, and the two-state model by the minimum and maximum values of the Ca^{2+} concentration c as a function of the IP_3 concentration p at $v_1=120/\text{s}$. For low values of IP_3, c settles at a stable

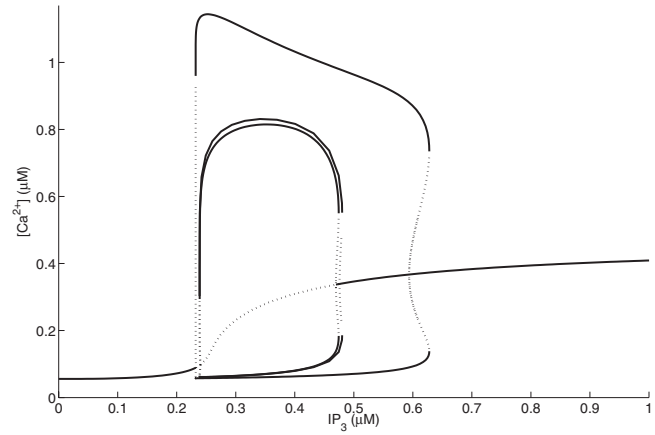

FIG. 4. The bifurcation diagram for the Ca^{2+} concentration c as a function of the IP_3 concentration for the six-state model, the four-state reduction, and the two-state reduction at $v_1=120$ and $c_{\text{ER}}=11$ μM. All other parameters are described in the text. Solid and dotted lines represent stable and unstable states, respectively.

equilibrium. The steady-state values of c increase as IP_3 is increased until the steady state loses stability via a subcritical Hopf bifurcation at $p=0.24$ μM. At this point, an unstable periodic orbit collapses onto the equilibrium, and both disappear. c is subsequently attracted toward a large-amplitude stable periodic orbit. The oscillations in c persist as p is increased until the same sequence of bifurcations occurs in reverse at $p=0.476$ μM. At this value of p, the unstable equilibrium undergoes a subcritical Hopf bifurcation, becoming stable, giving rise to an unstable periodic orbit whose amplitude quickly rises with increasing p. This orbit then collides with the large-amplitude stable periodic orbit at $p=0.628$ μM, and both orbits disappear in a saddle-node bifurcation of periodic orbits. For still higher values of p, c approaches the equilibrium values shown at the far right in Fig. 4. The second Hopf bifurcation at the larger IP_3 concentration occurs farther to the right for the two-state model and therefore, we do not further pursue the two-state reduction. Comparison of the bifurcation diagram of this two-state approximation (see Fig. 4) shows significant deviations from that of the full six-state model and four-state model and we therefore do not further this venue.

III. RESULTS

A single cluster of 20 IP_3Rs was simulated at the center of a 5×5 μm^2 grid, with an effective cytosolic Ca^{2+} diffusion coefficient of $D=25$ $\mu m^2\ s^{-1}$ at $IP_3=5$ μM. A typical Ca^{2+} puff has the spatial extent of about 2–4 μm. We record (a) the peak Ca^{2+} concentration at the site of the cluster, (b) the concentration averaged over a 1×1 μm^2 square centered at the puff site, and (c) the durations of the puffs in terms of the full width at half maximum (for a definition see Sec. III A). At this point, the Ca^{2+} concentration in the ER was chosen to be 11 μM and the flux constant v_{cluster} was chosen to be 5689/s, yielding peak maximum Ca^{2+} levels between 1 and 2 μM. We would like to mention here that almost identical results can be obtained by choosing a more realistic luminar calcium concentration of 500 μM but with a reduced value of about $v_{\text{cluster}}=200/\text{s}$. Stochastic opening

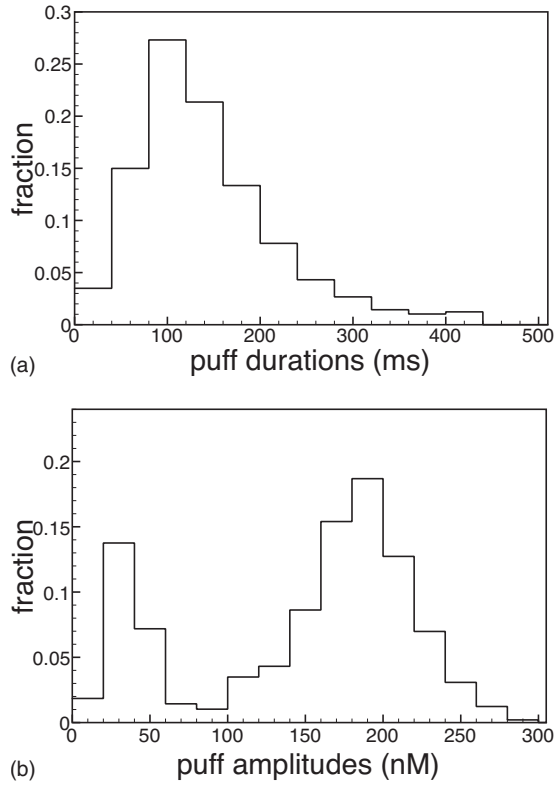

FIG. 5. Puff-amplitude (bottom panel) and puff-duration (top panel) distributions for the six-state model at $c_{ER}=11$ μM, $IP_3=5$ μM, and $v_{cluster}=5689/s$.

and closing of channels, within a cluster, gives rise to elementary Ca^{2+} release events with varying numbers of recruited channels.

A. Sequential protocol

We are using a sequential protocol, i.e., we continuously simulate the 5×5 μm^2 grid, generating thousands of sequential puffs. The puffs are characterized by their durations and their amplitudes, which are both statistically distributed since the number of channels recruited and their opening times are random. The puff amplitudes are defined as follows. A puff starts (at t_a) when more than one channel is open, corresponding roughly to an averaged Ca^{2+} concentration (averaged over a 1×1 μm^2 domain) of 20 nM above baseline. We do not consider at this point single-channel events but discuss them later. The puff ends at t_b, when the averaged Ca^{2+} concentration falls below 10 nM above baseline. The puff amplitude is defined as the maximum *averaged* amplitude within the time interval $[t_a,t_b]$. The duration of the puff is the time interval between the time the averaged Ca^{2+} concentration exceeds half the maximum for the first time and the last time within $[t_a,t_b]$. Experimental data obtained by various groups show puff lifetimes to be in the millisecond regime. Sun *et al.*[4] and Thomas *et al.*[24] reported puff lifetimes to peak at about 100 ms whereas Haak *et al.*[25] reported mean puff lifetimes of 60 ms.

In Fig. 5(a) we show the distribution of puff durations obtained by analyzing 5000 sequential puffs with our model at parameter values described above. The puff-duration distribution has a peak of around 100 ms, in excellent agreement with the experimental distribution, and average puff duration is about 150 ms.

Puff amplitudes show considerable variation, with values ranging from about 20 to 700 nM, as measured by Thomas *et al.*[24] In Fig. 5(b) we show the puff-amplitude distribution we obtained by averaging over 5000 sequential puffs at the same parameter values as above. Puffs generated had a minimum amplitude of about 16 nM and a maximum of about 300 nM, with a mean of 144.19 nM. The amplitude distribution we obtained also compares qualitatively with the distribution obtained in *Xenopus* oocytes by Sun *et al.*[4] [Fig. 8(A) therein], except for the large peak at small puff amplitudes. By analyzing this peak, we found that these peaks are predominantly due to two-channel events. Thus, in view of the absence of this peak in the reported experiments, it could be that either the experiments do not resolve all of these events (as suggested in Ref. 4) or that our model produces too many events where channel opening is poorly synchronized. Of all events observed, about 44% were single-channel events. An important factor for these large numbers of few-channel events is the sequential protocol as discussed below.

For a channel to activate, IP_3 binding is a prerequisite. Therefore puff properties vary with IP_3 concentrations. A very small IP_3 concentration fails to generate puffs, as not enough channels in the cluster have IP_3 bound. Increasing the IP_3 concentration increases the number of generated puffs as well as their amplitudes. We simulated 5000 sequential puffs and analyzed the puffs as described above. At $IP_3=0.5$ μM, we found for the rate of puffs (no single-channel events) about one puff in 750 s for their mean (averaged) amplitude about 50 nM and the duration of about 171 ms. Most of these events are few-channel events. As IP_3 is increased, the rate of puffs increases. For 5 μM IP_3, the puff rate is up to one puff in about 12 s, not counting single-channel events. Remarkably, the other properties, such as puff durations or puff amplitude, however, saturate once a certain level of IP_3 is reached. Between $IP_3=3$ μM and $IP_3=5$ μM, we have seen no change in the average puff durations and amplitudes, consistent with experimental conclusions.[5] As a matter of fact the entire distribution of puff durations and amplitudes is virtually unchanged between $IP_3=3$ μM and $IP_3=5$ μM.

B. Reduced models

As described above, the full six-state model for the IP_3 receptor may be reduced to a four-state and a two-state model using one or two quasi-steady-state approximations. While the four-state reduction seems most promising when the corresponding rate equations are compared, we have to also compare stochastic implementations of the reduced scheme, as the validity of the rate equation does not necessarily imply that for a stochastic implementation. In Fig. 6, we show the puff-duration and puff-amplitude distributions for the same parameters as above.

While overall, the four-state model works well, the six-state model gives us a mean lifetime of 157 ms and a mean amplitude of 144 nM. For the same set of parameters the four-state model gives us a mean lifetime of 135 ms and a

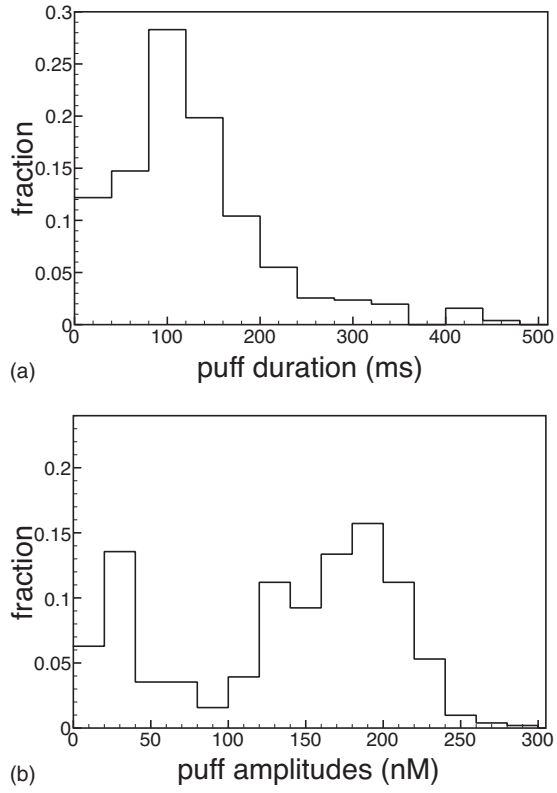

FIG. 6. Puff-amplitude (bottom panel) and puff-duration (top panel) distributions for $c_{ER}=11\ \mu M$, $IP_3=5\ \mu M$, and $v_{cluster}=5689/s$ but with the reduced four-state model for the IP_3 subunit described above.

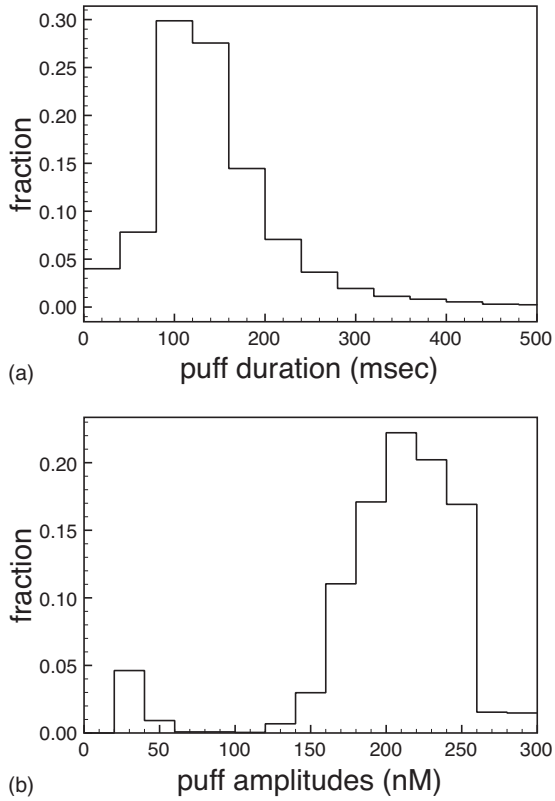

FIG. 7. Puff-amplitude (bottom panel) and puff-duration distributions (top panel) for $c_{ER}=11\ \mu M$, $IP_3=5\ \mu M$, and $v_{cluster}=5689/s$ obtained with the renewal protocol.

mean amplitude of 134 nM. This discrepancy in the mean values can be attributed to the larger number of small-amplitude events (20 nM) in the four-state model. This observation can be explained by the fact that in the four-state reduction we assumed equilibrium of IP_3 binding and disassociation to be instantaneous on the time scale of Ca^{2+} binding. Therefore, it is to be expected that IP_3 dissociates faster than the time it takes for Ca^{2+} activation to set in and thereby the failure to elicit a large puff. Correspondingly, the puff-duration distribution reveals a larger fraction of shorter puffs. For both models, puff durations peak at 100 ms while puff-amplitude distributions have a peak at 180–190 nM. The two-state reduction yields, as for the bifurcation diagram above, dissatisfactory answers (not shown) and is not further considered.

C. Renewal protocol

The above chosen protocol assumes that the puffs are generated sequentially and by one cluster only. In this section we use a protocol similar as in the computational study by Swillens *et al.*[26] We hold one channel open (the trigger channel), increasing the local Ca^{2+} concentration and thus the probability of puff initiation. Once the second channel opens, we release the trigger channel and record the emerging puff. When the averaged Ca^{2+} amplitude decreases below 5 nM above baseline, the puff is terminated and the system resets to prepuff conditions (i.e., the receptor states are re-equilibrized). The main motivation for using this protocol is that it eliminates correlations between puffs. If there is long-term inhibition, beyond the time interval between the puffs, puffs obtained sequentially (i.e., correlated puffs) are expected to exhibit different statistics than those obtained through the renewal protocol. We thus use the renewal protocol as a tool to detect correlations. If puff statistics are assembled from experiments by pooling puffs from different sites, temporal correlations are not present and the renewal protocol would be the protocol of choice for simulations.

For an IP_3 concentration of 5 μM and all parameters the same as above, we simulate 5000 decorrelated puffs analyzed the same way as described above. The resulting puff-amplitude and puff-duration distributions are shown in Figs. 7(a) and 7(b), respectively. The peaks around and below 50 nM amplitude are predominantly two-channel events. In comparison to the sequential protocol, the number of two-channel events is much smaller. The fraction of two-channel events is down from 16% to about 7%. For peak Ca^{2+} levels at the cluster site of the order $1-2\ \mu M$, the average fraction of open channels during a puff is slightly larger with the renewal protocol. Increasing the channel flux through IP_3Rs, so that peak Ca^{2+} concentrations at the cluster site are of the order of $10\ \mu M$, the average fraction of open channels remains about 50% in the renewal protocol, while it drops down to 25% in the sequential protocol, increasing the fraction of, e.g., two-channel events, while the fraction of two-channel events becomes virtually zero for the renewal protocol.

These results indicate (a) stronger channel synchrony during a puff in the renewal protocol than in the sequential

case (in particular, when local Ca^{2+} levels are high) and (b) correlations between successive puffs. Such correlations have been reported recently by Fraimann *et al.*[7] They recorded that a large puff amplitude is followed on the average by a large time interval to the next puff. Their analysis revealed that this correlation is due to a competition between inhibition (a long-term effect) and channel opening. The results reported here suggest the same hypothesis. A single-channel event shortly after a large-amplitude puff can recruit and synchronize only few, if any, other channels because of inhibition. For the same reason, the larger puffs [the peaks at large puff amplitudes in Fig. 5(a)] have a smaller amplitude in the sequential protocol (144 nM) versus the renewal protocol (200 nM) (compare the amplitude distributions in Figs. 5 and 7). The puff-duration distributions [see Fig. 7(b)] are similar in both protocols. The average puff duration with the renewal protocol is 147 ms (5000 puffs), in comparison to 157 ms in the sequential protocol. This correlates well with the differences in the puff amplitudes since larger amplitudes go often along with smaller durations for the increased inhibition at large puff amplitudes.

D. Local Ca^{2+} concentrations and maximum cluster flux

Computational modeling of a *single open channel*[9] and other work[26] suggest that the concentration of Ca^{2+} at the mouth of an open channel is of the order of 100 μM, decaying to fractions of 1 μM within 1 μm, giving rise to huge gradients of Ca^{2+} around the channel mouth which may affect the gating of the open channel and channels within the cluster. We found that for $c_{ER}=11$ μM, the value of $v_{cluster}$ of about 5000 generates puffs with the observed statistical properties. For the peak calcium concentration at the cluster site (not to be confused with the peak calcium concentration at the mouth of a channel) we find values of a few micromolars. If we targeted a cluster-site concentration of 100 μM, a concentration expected around a single channel,[10] we would clearly overestimate the influence of the channels on each other. In view of the analysis of the decay of the Ca^{2+} profile around the cluster in Ref. 10 and the assumption that channels are densely packed (around 10 nm distance) a few tens of micromolars seem reasonable as a target for the peak Ca^{2+} at the cluster site. If the channels are not as densely packed as suggested in Ref. 27 (300–800 nm cluster size), the cluster-site Ca^{2+} concentrations would be substantially smaller. To explore the effects of a large Ca^{2+} concentration at the cluster site (using the renewal protocol), we choose a realistic value of $c_{ER}=500$ μM but leave $v_{cluster}$ as large as $v_{cluster}=3000$ s^{-1}. All other parameters remain unchanged. The peak amplitudes at the cluster site are now about 25 μM on the average. The resulting distribution of puff amplitudes (averaged), however, peaks at almost 4 μM, a value much larger than in any experimental observation we are aware of. Furthermore, the distribution of puff lifetimes (see Fig. 8) peaks at about 20 ms, much less than in any experimental recording we are aware of. Most compelling, however, is the narrow range of the puff-duration distribution with essentially no puffs longer than 50 ms (see Fig. 8). Such characteristics are clearly inconsistent with observed puff durations.[3–5] For $c_{ER}=500$ μM and a smaller value for $v_{cluster}=1000/s$, the peak amplitudes at the cluster site are down to 10 μM on the average. The distribution of averaged puff amplitudes is 1.7 μM, still well beyond the experimental values we are aware of, and the puff-duration distribution peaks at about 30 ms, cutting off at about 70 ms.

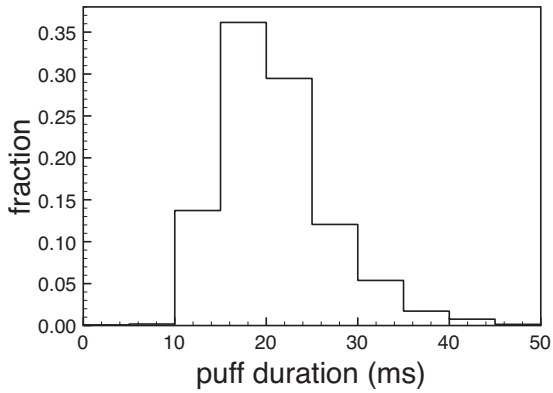

FIG. 8. Puff-duration distribution obtained with the renewal protocol for $c_{ER}=500$ μM and $v_{cluster}=3000/s$.

In order to match the statistics of the experimentally observed puffs, in amplitude, duration, and frequency, we are guided to a value for the maximum channel flux (at $c_{ER}=500$ μM) determined by a value for $v_{cluster}$ not more than about 300/s. We made a similar observation in an earlier work.[28]

IV. DISCUSSION

We put forward a simple *computationally inexpensive* model (six states and four states) for the IP_3 receptor which generates, in conjunction with a point-source approximation, calcium puffs with statistics in durations, averaged amplitudes, and frequencies consistent with numerous experiments. The model is derived from the DeYoung–Keizer model by requiring sequential binding of IP_3 and activating Ca^{2+} and an increased rate of inhibition. At the parameter values for $v_{cluster}$ and luminal Ca_{ER}, where we find good agreement between our model and experimentally observed puff statistics, the DeYoung–Keizer model with its original parameter values generates puffs that are generally much too long in duration (seconds) and too large in amplitude.

We have used two different protocols to generate puffs, a sequential protocol, where puffs are continuously generated from one cluster, and a renewal protocol, where we reset the conditions after the end of a puff to a predetermined state of the receptor subunits and basal Ca^{2+} levels (no channel open). The puffs generated by the renewal protocol exhibit generally a large fraction of open channels and a smaller number of few-channel events. The distribution of puff durations is similar in both protocols, while the distribution of puff amplitudes does not exhibit the large peak at small amplitudes due to the reduced number of few-channel events. This observation is consistent with puff correlations observed recently by Fraimann *et al.*[7] where puffs from a single-cluster site have been analyzed. As the differences be-

tween the two protocols increase for increasing Ca^{2+} concentrations at the cluster site, it is (like in Ref. 7) likely a consequence of inhibition.

Our model, however, at the parameter values that yield puff statistics consistent with experiments, generates peak Ca^{2+} concentrations of the order of about $1-2$ μM, *inconsistent* with other detailed computational studies[8–10] of single channels suggesting a concentration of tens of micromolars at the cluster-site Ca^{2+} (see Fig. 2 in Ref. 10). One way to reconcile the hypothesized large Ca^{2+} concentrations at the cluster sites in the range of tens of micromolars and the observed distributions of puff durations and averaged amplitudes on the micrometer scale may be dimensionality. Like in the Poisson equation in electrodynamics,[29] which is mathematically a similar problem as the diffusion of Ca^{2+} released by a point source, dimensionality is important. In one dimension, diffusion with a point source and a linear absorber (excessive buffer approximation) yields a *steady-state* profile which is finite at the cluster site and decays exponentially. In two dimensions, the concentration has a weak and very narrow logarithmic singularity at the cluster site. In three dimensions, the same setting yields a profile of the form $(1/r)\exp(-\alpha r)$,[30,31] with a seriously diverging Ca^{2+} concentration at the position of the source. While the diverging concentration at the cluster site (in one and two dimensions) is clearly a consequence of the steady-state source density, it is clear that in three dimensions, one would expect a larger peak concentration of Ca^{2+} at the cluster site.

With this observation in mind, we simulated our model in a 1 fl cube (mimicking experimental protocols). Simulation protocol is as described in the model section above. To obtain the averaged puff amplitudes, we average the Ca^{2+} concentrations over a cube of $(1\ \mu m)^3=1$ fl. For $c_{ER}=500$ μM and $v_{cluster}=3000/s$, we find an average peak Ca^{2+} concentration of about 130 μM, an average puff amplitude of about 1 μM, and an average puff duration of about 10 ms with little spread. None of the 500 simulated puffs had a duration longer than 30 ms. Next we use the much smaller value $v_{cluster}=125/s$ preserving the product $v_{cluster}c_{ER}$ we used in our two-dimensional model to generate puffs consistent with experimental recordings but with a more realistic luminal Ca^{2+} concentration of $C_{ER}=500$ μM. For these parameter values we find an average peak concentration of Ca^{2+} at the cluster site of about 10 μM, an average puff concentration of about 130 nM, and an average puff duration of about 100 ms, with a spread ranging from 2 to 300 ms. Remarkably, these results are similar to those we reported earlier for our two-dimensional model, except that the peak Ca^{2+} concentrations at the cluster site are more consistent with large Ca^{2+} gradients at the channel mouth.

This result suggests, that if one is interested in Ca^{2+} signaling phenomena on a larger spatial scale, i.e., in the collective dynamics of numerous cluster sites (but still based on accurate elemental event dynamics), a two-dimensional model *with moderate peak* Ca^{2+} *levels at the cluster sites* is more practical as it lacks the serious computational difficulties of the 3D models with huge Ca^{2+} gradients. What are lost in this approach are the accurate spatial details of the Ca^{2+} profiles well within the puffs, near cluster sites.

ACKNOWLEDGMENTS

We thank the National Science Foundation for support under Grant No. IOS 0345500.

[1] M. A. Pszczolkowski, W. S. Lee, H. P. Liu, and A. S. Chiang, Mol. Cell. Endocrinol. **158**, 163 (1999).
[2] Y. Yao, J. Choi, and I. Parker, J. Physiol. (London) **482**, 533 (1995).
[3] I. Parker, J. Choi, and Y. Yao, Cell Calcium **20**, 105 (1996).
[4] X. P. Sun, N. Callamaras, J. S. Marchant, and I. Parker, J. Physiol. (London) **509**, 67 (1998).
[5] H. J. Rose, S. Dargan, J. W. Shuai, and I. Parker, Biophys. J. **91**, 4024 (2006).
[6] I. Parker and Y. Yao, J. Physiol. (London) **491**, 663 (1996).
[7] D. Fraiman, B. Pando, S. Dargan, I. Parker, and S. P. Dawson, Biophys. J. **90**, 3897 (2006).
[8] S. Swillens, P. Champeil, L. Combettes, and G. Dupont, Cell Calcium **23**, 291 (1998).
[9] R. Thul and M. Falcke, Biophys. J. **86**, 2660 (2004).
[10] S. Rudiger, J. W. Shuai, W. Huisinga, C. Nagaiah, G. Warnecke, I. Parker, and M. Falcke, Biophys. J. **93**, 1847 (2007).
[11] G. Solovey, D. Fraiman, B. Pando, and S. Ponce Dawson, Phys. Rev. E **78**, 041915 (2008).
[12] Y. X. Li and J. Rinzel, J. Theor. Biol. **166**, 461 (1994).
[13] J. Keizer and G. DeYoung, J. Theor. Biol. **166**, 431 (1994).
[14] C. W. Taylor, P. C. A. daFonseca, and E. P. Morris, Trends Biochem. Sci. **29**, 210 (2004).
[15] G. W. De Young and J. Keizer, Proc. Natl. Acad. Sci. U.S.A. **89**, 9895 (1992).
[16] H. Tu, Z. Wang, and I. Bezprozvanny, Biophys. J. **88**, 1056 (2005).
[17] E. J. Kaftan, B. E. Ehrlich, and J. Watrass, J. Gen. Physiol. **110**, 529 (1997).
[18] D. O. D. Mak, S. McBride, and J. K. Foskett, Proc. Natl. Acad. Sci. U.S.A. **95**, 15821 (1998).
[19] J. Shuai, J. Pearson, J. Foskett, D. O. D. Mak, and I. Parker, Biophys. J. **93**, 1151 (2007).
[20] L. Ionescu, C. White, K.-H. Cheung, J. Shuai, I. Parker, and E. John, J. Gen. Physiol. **130**, 631 (2007).
[21] J. Shuai, J. Pearson, and I. Parker, Biophys. J. **95**, 3738 (2008).
[22] H. DeRemigio, J. R. Groff, and G. D. Smith, , IMA J. Math. Appl. Med. Biol. **25**, 65 (2008).
[23] J. R. Groff, H. DeRemigio, and G. D. Smith, in *Stochastic Methods in Neuroscience*, edited by C. Laing and G. Lord (Clarendon, New York, 2008).
[24] D. Thomas, P. Lipp, M. J. Berridge, and M. D. Bootman, J. Biol. Chem. **273**, 27130 (1998).
[25] L. L. Haak, L. S. Song, T. F. Molinski, I. N. Pessah, H. Cheng, and J. T. Russell, J. Neurosci. **21**, 3860 (2001).
[26] S. Swillens, G. Dupont, L. Combettes, and P. Champeil, Proc. Natl. Acad. Sci. U.S.A. **96**, 13750 (1999).
[27] J. Shuai, H. J. Rose, and I. Parker, Biophys. J. **91**, 4033 (2006).
[28] G. Ullah and P. Jung, Biophys. J. **90**, 3485 (2006).
[29] J. D. Jackson, *Electrodynamics*, 2nd ed. (Wiley, New York, 1975).
[30] G. D. Smith, J. Wagner, and J. Keizer, Biophys. J. **70**, 2527 (1996).
[31] G. D. Smith, Biophys. J. **71**, 3064 (1996).